Eurasian Journal of Anthropology
ISSN: 2166-7411

Euras J Anthropol 12(2):67-82, 2022

Understanding heat-induced changes in human bone remains using ATR-FTIR combined with chemometrics

Kameray Özdemir[1], Sevgi Haman Bayarı[2], Elif Hilal Şen[3], Cuauhtemoc Araujo-Andrade[4], Yılmaz Selim Erdal[1,5]

[1]Department of Anthropology, Hacettepe University, Ankara, Turkey

[2]Department of Physics Engineering, Hacettepe University, Ankara, Turkey

[3]Optician Program, Yüksek İhtisas University, Ankara, Turkey

[4]Unidad Academica de Fisica, Universidad Autonomo de Zacatecas, Zacatecas, Mexico

[5]Hacettepe University Skeletal Biology Lab (Husbio-L), Ankara, Turkey

Article info

Received: 28 April 2022

Accepted: 5 August 2022

Key words

Archaeological bone remains, Anatolia, burned bones, cremation, crystallinity

For correspondence

Kameray Özdemir

Department of Anthropology, Hacettepe University, 06800 Beytepe, Ankara, Turkey

E-mail:
kameray.ozdemir@hacettepe.edu.tr

Abstract

Physical and chemical properties of skeletal bone undergo significant alterations during burning. The analysis of heat-induced changes in human skeletal remains has been providing important knowledge that has been applied to the research of burned bones from archaeological and forensic settings. The study of burned bones is also fundamental to understand funerary behaviors. To understand heat-induced crystallinity changes in human bones, remains from five medieval sites in Turkey: Hakemi Use, Komana, İznik, Oluz Höyük and Tasmasor were burned under controlled conditions (from 300 to 900°C). Attenuated Total Reflectance Fourier Transform Infrared spectroscopy (ATR-FTIR) combined with Principal Component Analysis (PCA) was used to analyze the findings. Clear spectral differences were observed in the organic and inorganic components of the bone remains as a function of the temperature. Approximate cremation temperatures of cremated remains from Acemhöyük in Turkey were estimated using Partial Least-Square Regression (PLS).

Introduction

Bone is an impressive natural composite material consisting of a mineral phase (carbonated hydroxyapatite), an organic matrix (predominantly Type I collagen protein), and water (Weiner and Wagner, 1998; Grandfield et al., 2018; Von Euw et al., 2019). The molecular composition and crystalline structure of bone plays an essential role in its biological and structural functions (Weiner and Wagner, 1998).

The inorganic (mineral) component of bone is calcium-deficient nonstoichiometric biological apatite due to the presence of a substantial amount of anionic (e.g., HPO_4^{2-}, CO_3^{2-}, F^-, Cl^-) and cationic (e.g., Na^+, Mg^{2+}, K) species, together with the presence of ion vacancies in the crystal lattice (Elliot, 1994; White and Zhili, 2003). These substitutions modify the crystal lattice parameters (Boskey and Coleman, 2010; Roschger et al., 2008; Elliot, 1994; Rey et al., 2009; Oltza et al., 2007). To understand modification mechanisms and mineral recrystallization, crystallinity measurement is employed as an indicator of the degree of diagenetic change or thermal modification of bone mineral in archeological studies.

Fourier Transform Infrared spectroscopy (FTIR) is a rapid, powerful and non-destructive technique to investigate bone structure, diagenetic changes, and is particularly advantageous for analyzing thermally altered bone (Boskey and Mendelsohn, 2005; Lebon et al., 2008, 2010; Munro et al., 2007; Gonçelves et al., 2011; Snoeck et al., 2014; Bayari, 2012; Thomson et al., 2013; Ellingham et al., 2015; Piga et al., 2016; Legan et al., 2020; Mamede et al., 2017; Marques et al., 2018; Ellingham et al., 2016; Bayari et al., 2020). The infrared Crystallinity Index (CI_{FTIR}) or the Infrared Splitting Factor (IRSF) calculated from FTIR spectra of hard tissues is a widely used parameter to practically assess crystallinity (Weiner and Bar-Josef, 1990; Wright and Schwarcz, 1996).

The micro- and nano-structural changes of archeological bone are dependent on the presence of soft tissue (Ellingham et al., 2016; Nielsen-Marsh and Hedges, 2000; Trueman et al., 2004). This affects the crystallinity index and other spectral parameters obtained from the infrared spectrum. The crystallinity index increases with the chemical removal of organic components in buried and burned bones (Hedges, 2002; Dal Sasso et al., 2018). The effect of soft tissue on the bone and its decomposition pattern under the process of heating needs to be further investigated. Hence, systematic studies on the properties of unburned bone and an experimental set of data obtained for burned bone will allow us to understand heat-induced alterations in bone mineral structure and funerary behaviors (Piga et al., 2016; Thompson et al., 2009; Gonçalves et al., 2011; Mamede et al., 2017; Marques et al., 2018; Ellingham et al., 2016; Snoeck et al., 2014).

Burned human remains can be found on archaeological sites as a result of fire or a cremation process. Because cremation is one of the most common burial practices used by both present and past populations, researchers need to better understand the temperature and heating process. This will allow for a better comprehension of the modifications in bone structures due to combustion, and also to evaluate the differentiation between natural and anthropogenic phenomena (Piga et al., 2016; Thompson et al., 2009, 2011; Thompson and Chudek, 2007; Mamede et al., 2017; Efford, 2016; Snoeck et al., 2014).

Attenuated Total Reflectance Fourier Transform Infrared spectroscopy (ATR-FTIR) is one of the most powerful techniques for analyzing unburned, burned, and cremated bone remains (Surovell and Stiner, 2001; Chadefaux et al., 2009; Thompson et al., 2011; Hollund et al., 2013; Beasley et al., 2014; Piga et al., 2016; Dal Sasso et al., 2016; Bayari et al., 2020).

Chemical changes occurring in bone remains exposed to different temperatures can be monitored by non-invasive ATR-FTIR spectroscopy and combined with chemometric analyses can provide us with a more precise temperature range to determine the (cremation) temperature of cremated (and/or burned) samples. The present study focuses on the characterization of heat-induced (300-900°C) chemical changes in human bone remains from five archaeological sites in

Turkey. We then use this information to estimate the cremation temperature of cremated remains from the site of Acemhöyük.

Materials and methods

Osteological material and burial conditions

Rib fragments that did not exhibit any signs of pathology, trauma or modification (including burning), from sub-adult individuals aged 0 to 5 years old from sites dated to the medieval period were sampled for analysis in this study. Rib fragments were chosen as they can be considered to be expendable elements compared to other postcranial skeletal elements due to their lack of morphological characteristics. The unburned bone samples come from the sites of Tasmasor in Erzurum (N=10), Hakemi Use in Diyarbakır (N=19), Komana in Tokat (N=10), İznik in Bursa (N=15), and Oluz Höyük in Amasya (N=10). The cremated bone remains (N=13) are from Acemhöyük in Aksaray. A map showing the locations of the studied sites is given in Fig. 1. The skeletal remains are housed in the Hacettepe University Skeletal Biology Laboratory (HUSBIO-L).

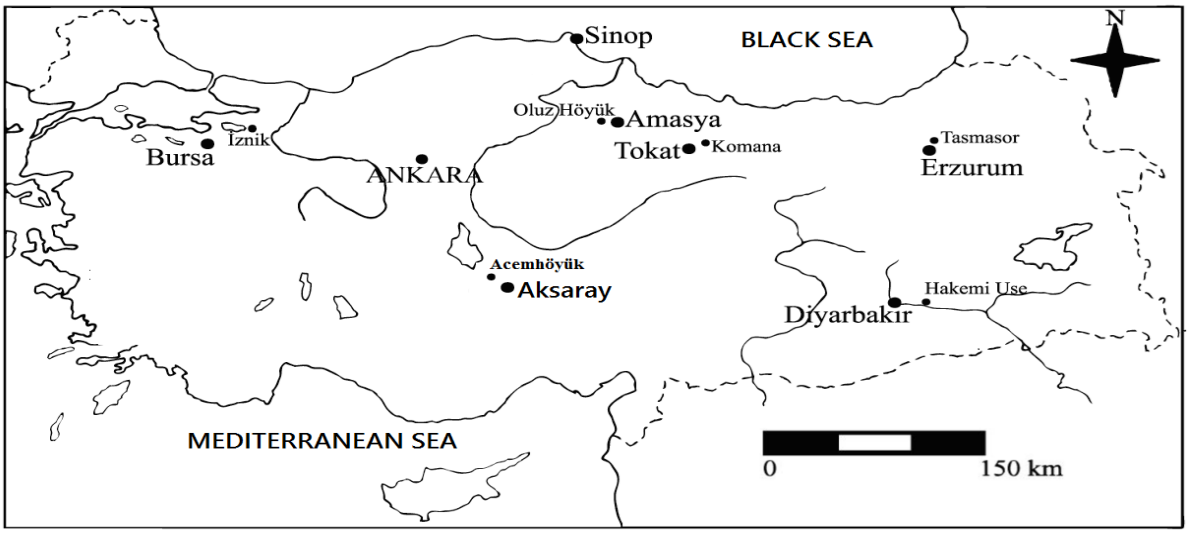

Figure 1. Skeletal element distribution for caprines each period

Tasmasor is located on geology comprised of volcanic tuff, agglomerate (volcanic breccias), and sedimentary rocks (Sözer, 1972), and the human bone remains were recovered from pits dug into areas composed of the soft volcanic tuff (Erdal, 2014). Hakemi Use is a multilayered hill site with occupational activities of prehistoric peoples from the Neolithic period to the Iron Age. The highest level of the *höyük* was used as a cemetery by medieval people (Erdal, 2013). The medieval graves at Hakemi Use were dug into soft soils containing humic substances. The presence of such a soil structure increases the contact of the bones with oxygen and limits preservation conditions. In addition, there is modern irrigation-based agricultural activity (cotton cultivation) in the region, and the area is adjacent to the Tigris River. Consequently, the soil in the area is characterized by high moisture content. The ancient city of Komana, a *höyük* site like Hakemi Use, is located in the floodplain on the banks of the Yeşilırmak River (Altın, 2015). The lowest level is parallel to the river and covered by metamorphic rocks (Altın, 2015). The skeletons were mostly recovered from graves that were carved into the metamorphic rocks. Oluz Höyük is 15 m higher than the level of the plain and was formed after the draining of a swamp (Özdemir et al., 2015). The skeletons were recovered from simple earthen graves. The İznik skeletons were recovered from the Roman theater, which was used as a dumping site for waste after the 8th

century AD and later as a cemetery in the Byzantine period (Yalman, 1994). Organic waste, animal bones, pottery sherds, and ash were deposited in the theater area for long time. The skeletons were recovered from brown humus soil above this landfill. Furnaces were constructed to make ceramic tiles in the same area during the Ottoman period (Yalman, 1994), and the region was later used as an agricultural area. Acemhöyük is located in central Turkey in the province of Aksaray at the intersection of main roads 18 km northwest of the modern town of Yeşilova (Durur, 2019). Aksaray city center to the south of the fault step where the Kızılırmak plateau and the Tuz Gölü (Salt Lake) basin are separated from each other. The archaeological site of Acemhöyük, is located in the closed basin of the Salt Lake of the Aksaray Plain, which is a large and fertile area irrigated by the Uluırmak River. Surrounded by the volcanic Hasan and Melendiz Mountains to the south, and the Ekecik and Tavşan Mountains to the northeast, Acemhöyük is situated quite close to the southern shore of the Salt Lake (Özgüç, 1968; Ekmen, 2012; Kamış, 2012). The mound of the actual site is about 700-600 m high with four high points and some flat areas. Excavations at Acemhöyük first began in 1962 under the direction of Nimet Özgüç and after 1989 they were continued under the direction of Aliye Öztan (Özgüç, 1968; Öztan, 1991, 2014). Acemhöyük had been settled and inhabited since the Chalcolithic and Early Bronze Ages, but its peak of occupation was during the Old Assyrian Colony Period, in the Middle Bronze Age.

The age-at-death of the individuals was previously determined through standard osteological methods (Table 1). The sex estimation of the adult skeletons was based on the macro examination of morphological features of the skull, pelvic girdle, and long bones (Buikstra and Ubelaker, 1994). The skeletal features used for determination of age-at-death for the adults were cranial suture closure, and macro examination of sternal rib end morphology, the pubic symphysis, and the auricular surfaces of the ilium (İşcan et al., 1984, 1985; Lovejoy et al., 1985; Meindle and Lovejoy, 1985; Buikstra and Ubelaker, 1994). The age-at-death of the sub-adults was assigned using dental development and skeletal element metrics, ossification development, and the degree of epiphyseal union (Asscher et al., 2011; Ubelaker, 1989). No sex estimation was performed for sub-adult individuals since sexual characteristics can only be observed following puberty.

Table 1. Demographic features of the studied samples. Infant = ≤1 year old; Child = 1-15 years old; Young Adult = 15-30 years old; Middle Adult = 30-45 years old; Old Adult = 45+ years old; Adult? = probable adult (>15 years old)

Number	Site	Skeletal Code	Sex	Age Group	Number	Site	Skeletal Code	Sex	Age Group
1	Tasmasor	TMS M48	Unknown	Infant-Child	39	İznik	İTK 89 53/7	Unknown	Child
2	Tasmasor	TMS M117	Unknown	Infant-Child	40	İznik	İTK 89 53/33	Unknown	Child
3	Tasmasor	TMS M164	Unknown	Infant-Child	41	İznik	İTK 89 53/27	Unknown	Infant-Child
4	Tasmasor	TMS M95	Unknown	Infant-Child	42	İznik	İTK 90 58/6	Unknown	Child
5	Tasmasor	TMS M100	Unknown	Infant-Child	43	İznik	İTK 90 58/1	Unknown	Child
6	Tasmasor	TMS M109	Unknown	Infant-Child	44	İznik	İTK 90 56/7	Unknown	Child
7	Tasmasor	TMS M115	Unknown	Infant-Child	45	İznik	İTK 90 56/2	Unknown	Child
8	Tasmasor	TMS M118	Unknown	Infant-Child	46	İznik	İTK 90 56/11	Unknown	Child
9	Tasmasor	TMS M129	Unknown	Infant-Child	47	İznik	İTK 90 56/10	Unknown	Child

10	Tasmasor	TMS M137	Unknown	Infant-Child	48	İznik	İTK 90 55/1	Unknown	Child
11	Hakemi Use	HKM'05-M-80-H8b	Unknown	Child	49	İznik	İTK 89 53/4	Unknown	Child
12	Hakemi Use	HKM'05-M-85-I8	Unknown	Child	50	İznik	İTK 89 53/21	Unknown	Child
13	Hakemi Use	HKM'05-M-86-G8b	Unknown	Child	51	İznik	İTK 89 53/19	Unknown	Child
14	Hakemi Use	HKM'06-M-167	Unknown	Child	52	İznik	İTK 89 53/1	Unknown	Child
15	Hakemi Use	HKM'06-M-173	Unknown	Child	53	İznik	İTK 89 41/5	Unknown	Child
16	Hakemi Use	HKM'08-M-244-G7	Unknown	Infant	54	Oluz Höyük	OLZ SK 50	Unknown	Infant-Child
17	Hakemi Use	HKM'08-M-257	Unknown	Child	55	Oluz Höyük	OLZ SK 64	Unknown	Infant-Child
18	Hakemi Use	HKM'12-M-443-I11	Unknown	Child	56	Oluz Höyük	OLZ SK 83	Unknown	Infant-Child
19	Hakemi Use	HKM'12-M-446-I12	Unknown	Child	57	Oluz Höyük	OLZ-07 SK-7	Unknown	Infant-Child
20	Hakemi Use	HKM'12-M-436-G8	Unknown	Child	58	Oluz Höyük	OLZ-07 SK-8	Unknown	Infant-Child
21	Hakemi Use	HKM'11-M-406	Unknown	Child	59	Oluz Höyük	OLZ-07 SK-11	Unknown	Infant-Child
22	Hakemi Use	HKM'11-M-392-F8	Unknown	Child	60	Oluz Höyük	OLZ-08 SK-19	Unknown	Infant-Child
23	Hakemi Use	HKM'11-M-387-F8	Unknown	Infant	61	Oluz Höyük	OLZ-09 SK-32	Unknown	Infant-Child
24	Hakemi Use	HKM'12-M-424-b-H12	Unknown	Child	62	Oluz Höyük	OLZ-11 SK-57	Unknown	Infant-Child
25	Hakemi Use	HKM'12-M-526-H12	Unknown	Child	63	Oluz Höyük	OLZ-12 SK-112	Unknown	Infant-Child
26	Hakemi Use	HKM'12-M-517-b-I12	Unknown	Child	64	Acem Höyük	Acem 93 M3	Female	Adult?
27	Hakemi Use	HKM'12-M-458-a-I11	Unknown	Infant	65	Acem Höyük	Acem 93 M8	Male	Adult?
28	Hakemi Use	HKM'05-M-57b-2	Unknown	Child	66	Acem Höyük	Acem 93 M12	Male	Middle Adult
29	Hakemi Use	HKM'02-M-8-E10	Unknown	Child	67	Acem Höyük	Acem 95 M32	Female	Middle Adult
30	Komana	HTP 01 G04	Unknown	Child	68	Acem Höyük	Acem 95 M37	Female	Young Adult

31	Komana	HTP 01 282/598 T05	Unknown	Infant	69	Acem Höyük	Acem 95 M47	Male	Middle Adult
32	Komana	KARP 11 252/613-A	Unknown	Child	70	Acem Höyük	Acem 95 M41	Male	Middle Adult
33	Komana	HTP 02 G17/A	Unknown	Child	71	Acem Höyük	Acem 95 M50	Female	Adult?
34	Komana	HTP 02 G 23	Unknown	Child	72	Acem Höyük	Acem 95 M59	Male	Middle Adult
35	Komana	HTP 01 G16	Unknown	Child	73	Acem Höyük	Acem 95 M65	Female	Young Adult
36	Komana	HTP 02 G20 E	Unknown	Child	74	Acem Höyük	Acem 95 M68	Male	Middle Adult
37	Komana	KARP 13 HTP 01 G45 267/603 T09	Unknown	Infant	75	Acem Höyük	Acem 95 M77	Male	Adult?
38	Komana	KARP13 HTP01 277/613 G57 T 014	Unknown	Infant	76	Acem Höyük	Acem 96 M33	Female	Young Adult

The burning process

Bone remains were exposed to burning at different temperatures to eliminate the effect of the organic component on the CI_{FTIR}. For that purpose, we followed the experimental procedures outlined by Person et al. (1996) to produce controlled crystallinities. Bone sections were then rinsed in an ultrasonic bath with distilled water before they were air-dried. Five sections of the bones from each archeological site were placed in heat resistant ceramic crucibles and placed in a furnace (Protherm PLF 100/3**)** for 3 hours at fixed temperatures; 300, 500, 700 and 900°C. The oven was then switched off and its internal atmosphere was allowed to cool for a further 5 hours.

Changes in bone color have previously been demonstrated as an indicator for estimating the burning/cremation temperature of bones (Ellingham et al., 2015, 2016). After cooling, the samples were photographed and the color of each sample (Fig. 2) was assigned using a Burn Color Code developed by Stiner et al. (1995) and the Munsell Soil Color Chart (GretagMacbeth, 2020).

Figure 2. Coloring of human bone remains heated from 25 to 900°C. The color codes refer to those of the Munsell Color system (GretagMacbeth, 2020).

ATR-FTIR spectroscopy and spectral analysis

ATR-FTIR spectra were recorded for the powdered bone remains (1 mg) using a Perkin Elmer Spectrum, with one FTIR spectrometer equipped with a deuterated triglycine sulfate (DTGS) detector with a monolithic diamond ATR accessory (Pike Technology Inc., Madison WI). A total of 32 scans were performed for all measurements with a resolution of 4 cm^{-1} in the 4000-450 cm^{-1} spectral regions. The strong Norton-Beer apodization function was used for processing the interferogram. Five measurements were made on each sample to check the reproducibility of the identical spectra. The average spectra were smoothed using a Savitzky-Golay filter (polynomial order 9) and then the baseline was corrected using OPUS 5.5 software (Bruker Optics GmbH, Ettlingen, Germany).

The Crystallinity Index (CI) applied here in this study is the same as that used in archaeological and forensic applications. To obtain the CI_{FTIR} values, the band intensities (the peak height) of the two absorption bands around 563 cm^{-1} and 603 cm^{-1} (v_4 phosphate antisymmetric bending vibrations) were added and divided by the height (around 590 cm^{-1}) of the minimum between them, after baseline correction from 700 to 500 cm^{-1} (Weiner and Bar-Yosef, 1990; Surovell and Stiner, 2001; Piga et al., 2016; Bayari et al., 2020).

The band at around 1417 cm^{-1} (v_3 carbonate band) is ascribed to the B-type carbonate and has been identified as a spectral marker of heat-induced changes in bone (Thompson, 2009; Lebon et al., 2010, 2011; Hollund, 2013; Grunenwald et al., 2014; Snoeck et al., 2014; Mamede et al., 2017; Marques et al., 2018; Gonçalves et al., 2018; Piga et al., 2016). This band is generally used to obtain the carbonate to phosphate ratio (C/P), which quantifies the relative amount of

B-type carbonate in apatite. In this study, the C/P ratio is obtained by dividing the height of the v_3 carbonate band by the height of the v_3 phosphate band.

Principal component analysis (PCA) and partial least square (PLS) analysis

PCA is an unsupervised multivariate statistical method commonly used to reduce the number of predictive variables and solve the multi-collinearity problem. It is applied without the consideration of the correlation between the dependent variables and the independent variables (Esbensen, 2005).

PLS is a supervised dimension reduction multivariate methodology allowing for the calibration of prediction models by relating the variations in one or several response variables (Y-variables) to the variations of several predictors (X-variables). PLS is a bilinear modeling method where information in the original X-data is projected onto a small number of "latent variables" called PLS-components. The Y-data are used for estimating the latent variables, ensuring that the first components are the most relevant for predicting the unknown Y-variables (Esbensen, 2005).

The ATR-FTIR data for the studied bone remains were imported into The Unscramble X10.3 (CAMO Software Inc. Oslo, Norway). PCA was applied to the second derivative and vector normalized data. PCA was performed for the 4000 to 450 cm^{-1} spectral region for all groups. Multivariate calibration of PLS was performed using the same software employing the original spectra and the first and second derivative-transformed spectra. All predicted values are accompanied by a statistical parameter coefficient of determination, R-square, the root mean square error of prediction (RMSEP), and bias (the average value of the difference between predicted and measured values) which accounts for the reliability of the prediction.

Results

ATR-FTIR spectra and crystallinity index

A representative ATR-FTIR spectrum (Fig. 3A) of unburned human bone remains from Hakemi Use exhibits common vibrational bands corresponding to the organic and mineral components of bone/bone remains (Mamede et al., 2017; Marques et al., 2018; Gonçalves et al., 2018; Boskey and Pleshko-Camacho, 2007; Lopes et al., 2018; Elliot, 1985; Bayari et al., 2020).

The weak band around 1660 cm^{-1} is attributed to the absorption of the Amide I (peptide bond, mainly C=O, stretching vibration of the collagen matrix), which represents the organic matrix of bone. The phosphate moiety in HA gives rise to the bands in two different spectral regions. The P–O symmetric and asymmetric stretching vibrations (v_1 and v_3) occur in the 900-1200 cm^{-1} spectral region as a broad band whereas the v_4 asymmetric P-O bending vibration gives rise in two distinct bands in the 500-700 cm^{-1} region. The strong band at 1020 cm^{-1} can be attributed to v_3 (PO_4^{3-}) vibration in non-stoichiometric apatite that contains CO_3^{2-} and/or HPO_4^{2-} (Rey et al., 1991). The phosphate v_1 band was also observed as a shoulder at ca. 960 cm^{-1}. The bands around 1450 cm^{-1} (A-type carbonated apatite) and 1417 cm^{-1} (B-type carbonated apatite) were assigned to a v_3 vibrational mode and the band at 872 cm^{-1} (B-type carbonated apatite) is due to the v_2 vibrational mode of carbonate ions (Elliot, 1985; Rey et al., 1991; Lebon et al., 2011; Marshall and Marshall, 2015).

Fig. 3B shows the spectral changes of the average ATR-FTIR spectra of human bone remains from Hakemi Use as a function of temperature values (unburned-25°C, 300°C, 500°C, 700°C and 900°C). The average ATR-FTIR spectrum of cremated human remains from Acemhöyük is also given in this figure.

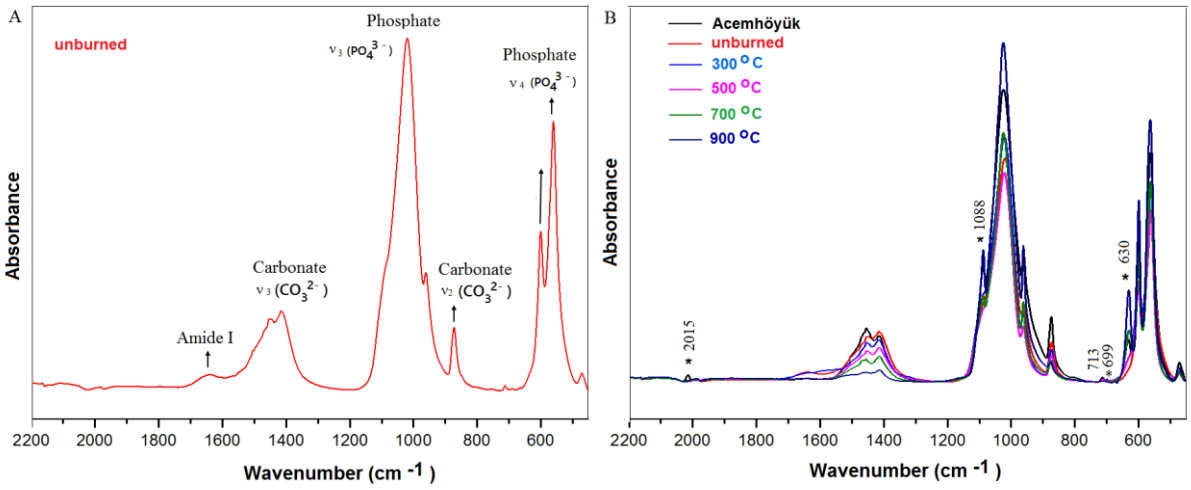

Figure 3. The representative average ATR-FTIR spectrum with assignments of main bands of human bone remains from Hakemi Use site (A). Baseline-corrected ATR-FTIR spectra of human bone remains from Hakemi Use site as a function of temperature and cremated bone remains from Acemhöyük site in the 1800-450 cm^{-1} spectral region (B).

At temperatures between 25 and 300°C, no pronounced differences are apparent between the ATR-FTIR spectra of the unburned and burned bone remains. The absorbance value of the Amide I band of organic matrix (mainly collagen) decreases, the organic matrix began to decompose at a temperature around 300°C, and the complete decomposition of the organic component coincides with the recrystallization of bone mineral (calcined bone) after 700°C.

The phosphate band at 1020 cm^{-1} shifts to higher wavenumbers after 700°C and indicates modifications in the phosphate ion environments during heating. New bands in the spectra appear at about 3574, 1088, and 630 cm^{-1} after 500°C.

The band at 630 cm^{-1} (in plane bending vibration of OH^- group), present in the ATR-FTIR spectra of bone remains at 700°C, originates from the decomposition of the phosphate by the liberation of OH^- group. A-type carbonates are lost and the crystallinity of the bone mineral is increased (Thomson et al., 2009).

Appearance of the ▫3 phosphate band at 1088 cm^{-1} in the ATR-FTIR spectra of the burned (and cremated) bone remains is due to an increase of the apatite crystal size, which causes the v_1 and v_3 phosphate bands to become more resolved and the structure is similar to that of the stoichiometric apatite. This band can also be associated with an F-substituted apatite marker (Trueman and Tuross, 2002; Bayari et al., 2020).

The additional bands at 2015, 713, and 699 cm^{-1} were observed in the ATR-FTIR spectra of the cremated human bone remains from Acemhöyük. The bands at 2015 cm^{-1} and 699 cm^{-1} are related to the formation of cyanamide apatite, $Ca_9(PO_4)_5(HPO_4)(HCN_2)$, under an ammonia atmosphere. We did not observe this band in the ATR-FTIR spectra of the burned bone remains, and this band may be used as an indicator for true cremation processes (Dowker and Elliot, 1979; Van Strydonck et al., 2010; Zazzo et al., 2013).

In the light of the spectral similarity, we propose that the cremation temperature of the cremated remains from Acemhöyük was above 700°C. The band at 713 cm^{-1} is due to the formation of calcite in cremated bone remains that could come from the absorption of atmospheric CO_2 by calcium oxide (CaO), which forms above 700▫C (Rogers and Daniels, 2002). A calcite band is also observed in the ATR-FTIR spectra of unburned bone remains from Hakemi Use and Tasmasor. The integrated intensities of the two absorption bands around 563 cm^{-1} and

603 cm^{-1} (v_4 phosphate antisymmetric bending vibrations) in the wavenumber region (500-700 cm^{-1}) significantly increase with temperature (Fig. 4A).

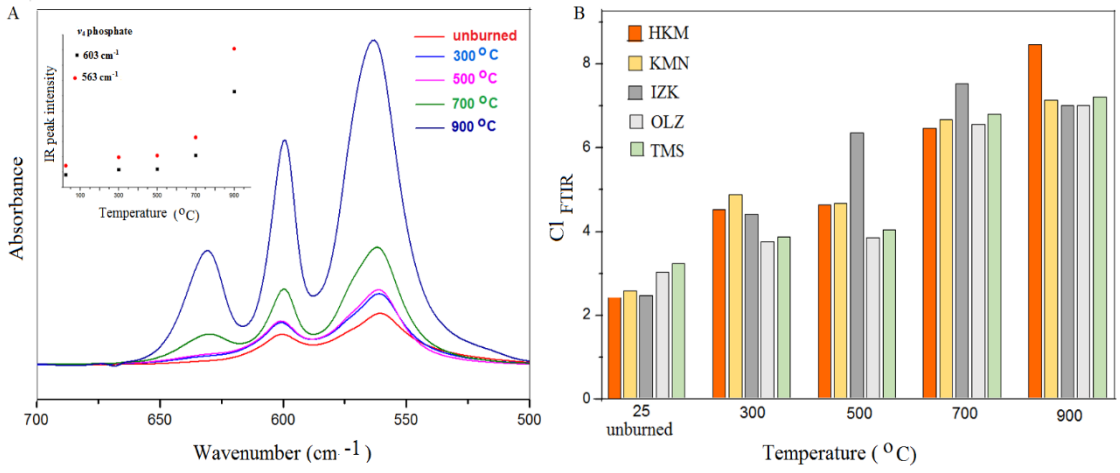

Figure 4. ATR-FTIR spectra of bone remains from Hakemi Use site in the v_4 phosphate wave number region (500-700 cm^{-1}) as a function of temperature. The inset shows the variation of the integrated intensities of two bands in this spectral region as a function of temperature (A). Crystallinity index (CI_{FTIR}) variation of unburned and burned human bone remains from five sites as a function of temperature. Abr. OLZ (Oluz Höyük), TMS (Tasmasor), HKM (Hakemi Use), KMN (Komana) and IZK (İznik).

As seen from Fig. 4B, the CI_{FTIR} index increases from 2.5 to 3.3 in unburned bone remains from the five sites (at room temperature) to ca. 7.1 to 7.3 (except Hakemi Use; 8.6) at 900°C which reveals that the mineral phase is similar to that of stoichiometric crystalline carbonated hydroxyapatite. This was also clearly revealed by the band narrowing and by the noticeable sharper bands observed in the 500-700 cm^{-1} spectral region after 700°C (Fig. 4A).

An increased degree of CI_{FTIR} index for higher temperatures is consistent with the loss of carbonate (see the ▫$_2$ and ▫$_3$ carbonate bands in Fig.2B), water and organic components and causes a rearrangement of the apatite structure. This result is related to an increase in crystal size that also becomes more ordered (Weiner and Bar-Yosef, 1990; Dal Sasso et al., 2018; Marques et al., 2018).

The carbonate to phosphate ratio (data not shown) decreased significantly with increasing temperature, which reveals the formation of a more stable mineral phase. The main reason for this is the increasing proportion of the inorganic fraction following loss of the organics as a result of the heating process (Asscher et al., 2011; Nielsen-Marsh and Hedges, 2000; Person et al., 1996; Stathopoulou et al., 2008; Surovell and Stiner, 2001; Thompson et al., 2009).

The color changes that occur in bone during heating/cremation are because of the combustion of the organic matrix and depend on bone crystallinity. The temperature estimation can be achieved when taking into account a quantitative technique such as the infrared band intensity or area ratio analyses, as well as qualitative data such as the bones' color (Piga et al., 2016; Thompson and Chudek, 2007; Thompson et al., 2011; Mamede et al., 2017; Efford, 2016; Snoeck et al., 2014; Marques et al., 2018). The Munsell Color index (GretagMacbeth, 2020) and the Burn Color Code developed by Stiner et al., (1995) can assess the degree of calcination of bone. Based on the color changes in the human bone remains studied in this study (Fig. 2) show that the bone calcined (white color which is the natural color of hydroxyapatite) at 900°C and the bone is then only comprised of the inorganic fraction (bone apatite).

PCA results

In order to evaluate the spectral differences between bone remains, PCA was conducted on the infrared spectral data set. As observed in Fig. 5 (A and B), human bone remains from Oluz Höyük and Tasmasor cluster away from the rest of samples at temperatures equal to or below 500ºC. This behavior is similar to that observed previously for unburned bone remains (Bayari et al., 2020).

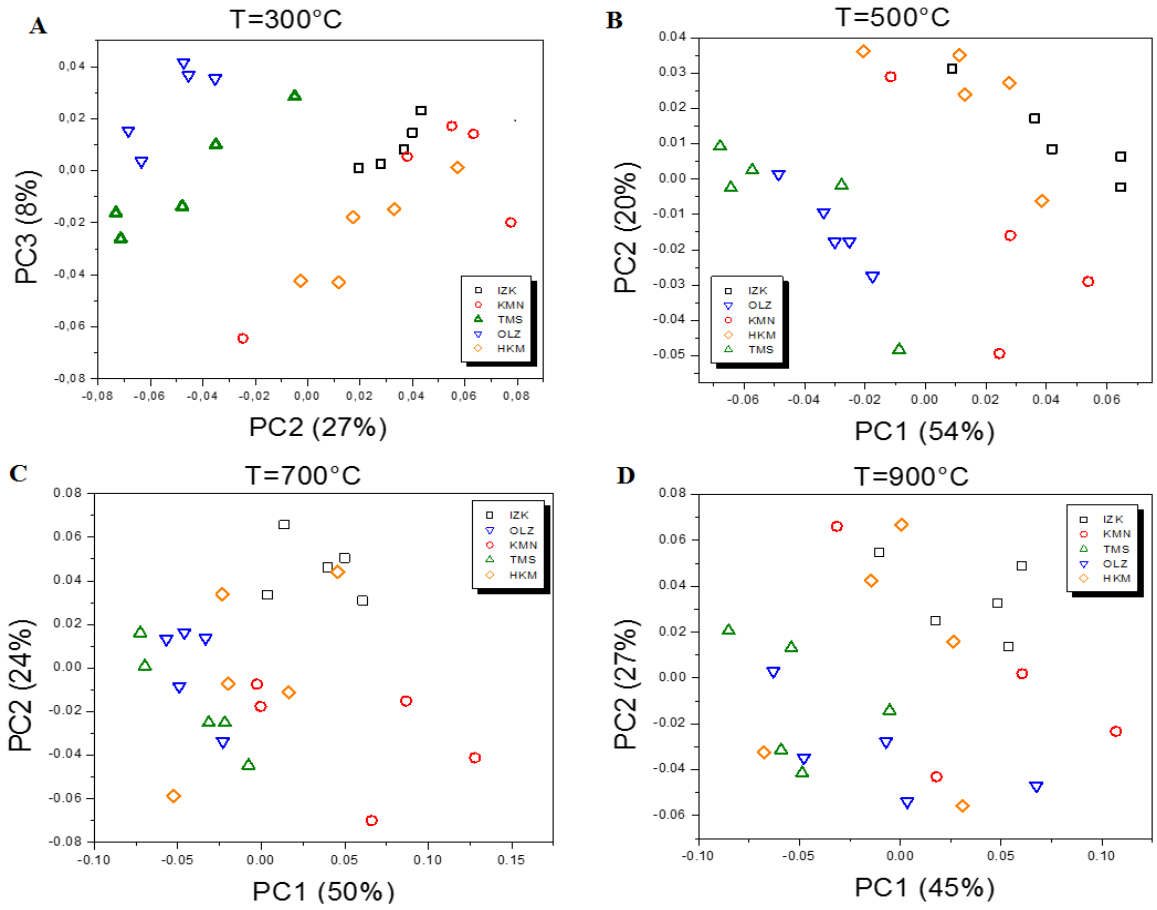

Figure 5. PCA-scores plot (PC2 x PC1) for the burned human bone remains from the five archaeological sites analyzed in this study at different temperatures (300°C to 900°C). Abr. OLZ (Oluz Höyük), TMS (Tasmasor), HKM (Hakemi Use), KMN (Komana) and IZK (İznik).

This indicates that at these ranges of temperatures, significant changes in the physical-chemical properties of the human bone remains do not exist. On the other hand, when temperature increases to *ca*. 700ºC and higher, it is no longer possible to identify any clustering in the score plots depicted in Fig. 5 (C and D). This result confirms the fact that homogenization in the chemical composition and crystalline structure of the bone samples occurs, as well as decomposition in the organic matrix of collagen.

PLS-models and estimating cremation temperature

PLS-models were calibrated in order to predict the cremation temperature of the cremated remains from Acemhöyük. Initially, five models were calibrated using the FTIR-ATR spectra collected from the bone remains from the five archaeological sites at 300, 500, 700, and 900ºC. After evaluating the statistical values of each model, only those calibrated with the spectra of

human bone remain from Hakemi Use (Fig. 6A) and Komana (Fig. 6B) showed the highest *R-square* values and lowest RMSEP values. The lower the RMSEP value, the better the prediction power of the developed calibration model.

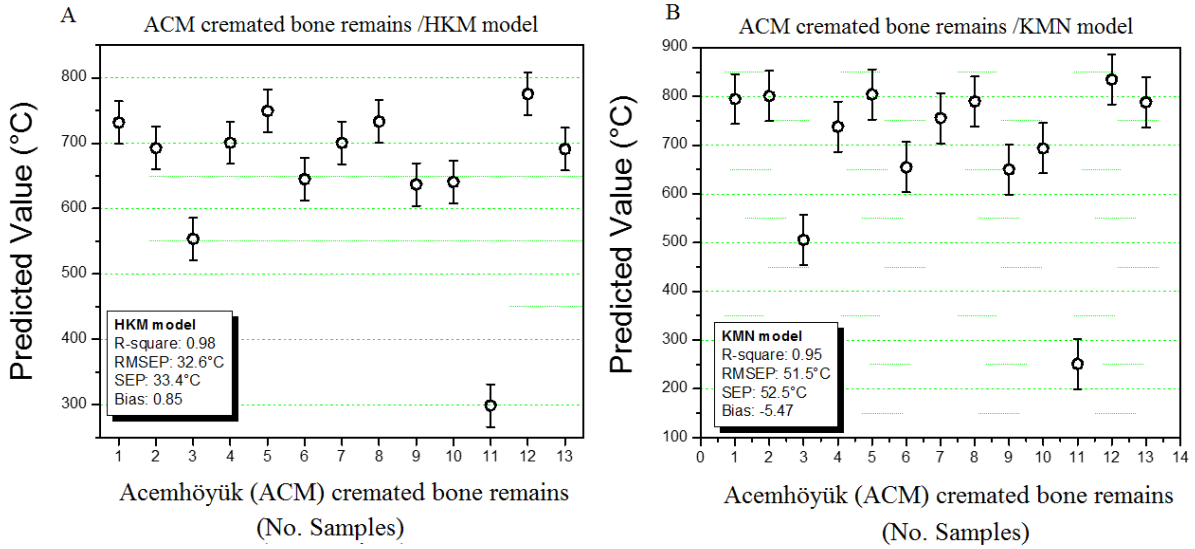

Figure 6. PLS model predicted values (ºC) for cremated bone remains from Acemhöyük. Model calibrated using bone remains from Hakemi Use (HKM) site (A). Model calibrated using bone remains from Komana (KMN) (B). The error bars correspond to the RMSEP values computed for each model.

Predictions obtained for both models, depicted in Figure 6 (A and B), indicate that the cremation temperature of the cremated remains from Acemhöyük were likely between 700 and 800 ºC.

Discussion and conclusions

Understanding thermally induced changes of burned bone remains are very important in forensic science and archeology. The estimation of the temperature affecting skeletal remains (burned or cremated) has previously been attempted via infrared spectroscopy (Ellingham et al., 2015; Mamade et al., 2018; Marques et al., 2018; Snoeck et al., 2014; Legan et al., 2020). Several infrared indices such as infrared crystallinity index (CI_{FTIR}), A or B carbonate to phosphate index for carbonate content, C/P, OH/P band intensity or area ratios have been proposed for the study of burned and cremated bone. These indices were identified as those which displayed clear quantitative relationships with temperature revealing heat-induced changes.

Mamade et al. (2018) used three type OH/P intensity ratios as an infrared spectral marker based on OH liberation at 630 cm^{-1} from hydroxyapatite, a ν(OH) stretching band at ~3570 cm^{-1}, and a $\nu_4(PO_4^{3-})$ band at 603 cm^{-1} to identify burned bones at high temperatures (>800 °C) and to discriminate differences between fossilized and burned archeological bones. Snoeck et al. (2014) investigated the carbonate content and CI index of experimentally heated samples and archaeological cremated remains and suggested that FTIR yields information about the heating conditions. Lagan et al. (2020) estimated burning temperature from total reflection FTIR spectra of cremated human remains from different Slovenian archaeological sites using spectral alterations from experimentally heated bone. They found that the temperature during the cremation process was between 600 and 900 ºC.

In this study, burned (under a controlled environment) and cremated bone remains were analyzed by ATR-FTIR spectroscopy with chemometric methods in order to evaluate the alteration of the molecular/structural properties. The effect of the burning temperature on the mineral component of bone remains; apatite crystallinity (CI_{FTIR}) values were calculated. The value of CI_{FTIR} that increases with temperature also occurs as a result of natural diagenetic processes (Surovell and Stiner, 2001). However, the CI_{FTIR} index did not linearly increase with temperature in any of the bone remains from the five different sites (Fig. 4). The most prominent spectral changes took place at 500°C and above. In previous FTIR studies on human bone it was documented that the organic component survived until temperatures of 400 ºC and is lost after 500ºC. At 600ºC the bones slowly begin to change color and the bone mineral is recrystallized (Holden, 1995; Thompson et al., 2013; Ellingham et al., 2015; Legan et al., 2020). When archaeological bone is heated it may possibly be due to an increased number of different foreign ions becoming improperly incorporated within the lattice of the recrystallized apatite. The spectral characteristics and heat-induced changes of burned bone remains from the five archeological sites were used to estimate the cremation temperature for cremated bone remains from Acemhöyük. A PLS multivariate method based on the ATR-FTIR spectra data demonstrates that the temperature during cremation was between 700 and 800 ºC.

The analysis of burned bone remains by ATR-FTIR spectroscopy is a low-cost, non-destructive, and rapid method requiring very small amounts of bone and no sample preparation. The use of these methods would allow for an insight into the cremation process and its effects on human bone from forensic contexts. Furthermore, it is also helpful to apply these methods before commencing with the stable isotopic and/or aDNA analysis studies as a control test mechanism when only burned bones are available for sampling before wasting time and money on the further biomolecular analyses. The analysis of heat-induced changes in bone can also provide valuable information about funerary processes. We also recommend that further studies with larger samples size be performed with, and without, the presence of soft tissue to further develop this method and elaborate upon the results obtained so far.

Declaration

The authors declare no conflict of interest. Data is available on request from the corresponding author.

Author statement

Kameray Özdemir: Conceptualisation; Methodology; Formal analysis, Investigation, Data Curation; Writing - Original Draft; Writing - Review and Editing; Visualisation; Project administration. Sevgi Haman Bayarı: Conceptualisation; Methodology; Formal analysis, Investigation, Data Curation; Writing - Original Draft; Writing - Review and Editing; Visualisation; Project administration. Elif Hilal Sen: Investigation. Cuauhtémoc Araujo-Andrade: Formal analysis. Yılmaz Selim Erdal: Resources; Review and Editing.

Funding

This study was supported by the Scientific and Technological Research Council of Turkey (TUBITAK, project number: 114K272) and Hacettepe University, Scientific Research Projects Coordination Unit (BAB, project number: FDS-2015-8623).

Acknowledgements

We would like to thank Dr. Benjamin Irvine of ANAMED (Koç University Research Center for Anatolian Civilizations) for editing the English of the manuscript.

References

Altın BN. (2015) Komana Ortaçağ yerleşimi/The medieval settlement at Komana. In: Erciyas B, Tatbul MN, editors. Komana antik kenti (Tokat) ve çevresinde jeoarkeolojik ve jeomorfolojik gözlemler. İstanbul: Ege Yayınları.

Asscher Y, Regev L, Winer S, Boaretto E. (2011) Atomic disorder in fossil tooth and bone mineral: an FTIR study using the grinding curve method. Archeosciences 35:135-140.

Bayari Haman S. (2012) Applications of vibrational spectroscopy in diagnosis and screening of dental tissues. In: Severcan F, Haris PI (editors). Vibrational spectroscopy in diagnosis and screening. Portland, OR: IOS press.

Bayari Haman S, Özdemir K, Sen EH, Araujo-Andrade C, Erdal YS. (2020) Application of ATR-FTIR spectroscopy and chemometrics for the discrimination of human bone remains from different archaeological sites in Turkey. Spectrochim Acta A Mol Biomol Spectrosc 237:118311.

Beasley MM, Bartelink EJ, Taylor L, Miller RM. (2014) Comparison of transmission FTIR, ATR, and DRIFT spectra: implications for assessment of bone bioapatite diagenesis. J Archaeol Sci 46:16-22.

Boskey AL, Mendelsohn R. (2005) Infrared analysis of bone in health and disease. J Biomed Opt 10(3):031102.

Boskey AL, Pleshko Camacho N. (2007) FT-IR imaging of native and tissue-engineered bone and cartilage. Biomaterials 28(15):2465-2478.

Boskey AL, Coleman R. (2010) Aging and bone. J Dent Res 89(12):1333–1348.

Buikstra JE, Ubelaker DH. (1994) Standards for data collection from human skeletal remains. Arkansas Archeological Survey Research Series No. 44, Arkansas.

Chadefaux C, Anne-Solenn LH, Bellot-Gurlet L, Reiche I. (2009) Curve- Fitting Micro –ATR- FTIR studies of the amide I and II bands of type I collagen in archaeological bone materials. E-Preservation Science 6:129-137.

Dal Sasso G, Lebon M, Angelini I, Lara Maritan L, Usai D, Artiolo G. (2016) Bone diagenesis variability among multiple burial phases at Al Khiday (Sudan) investigated by ATR-FTIR spectroscopy. Palaeogeogr Palaeoclimatol Palaeoecol 463: 168-179.

Dal Sasso G, Asscher Y, Angelini I, Nodari L, Artioli G. (2018) A universal curve of apatite crystallinity for the assessment of bone integrity and preservation. Sci Rep 8(1):12025.

Dowker SEP, Elliott JC. (1979) Infrared absorption bands from NCO− and NCN2− in heated carbonate-containing apatites prepared in the presence of NH_4^+ ions. Calcif Tissue Int 29(1): 177-178.

Durur ML. (2019) Acemhöyük ve Arıbaş mezarlığı'ndan insan iskelet kalıntılarının gömü geleneği açısından incelenmesi. MSc, Hacettepe Üniversitesi, Ankara, Turkey (Unpublished MA thesis, in Turkish with an abstract in English).

Efford M. (2016) The Implications of thermogenic modification for anthropological recovery of burned bone.

Ellingham STD, Thompson TJU, Islam M, Taylor G. (2015) Estimating temperature exposure of burnt bone-A methodological review. Sci Justice 55:181-188.

Ellingham STD, Thompson TJ, Islam M. (2016) The effect of soft tissue on temperature estimation from burnt bone using Fourier Transform Infrared Spectroscopy. J Forensic Sci 61(1):153-159.

Elliott JC. (1994) Structure and Chemistry of the Apatites and Other Calcium Orthophosphates. Amsterdam: Elsevier.

Elliot JC, Holcomb AW, Young RA. (1985) Infrared determination of the degree of substitution of hydroxyl by carbonate ions in human dental enamel. Calcif Tissue Int 37(4):372-375.

Ekmen H. (2012) Acemhöyük'te Asur ticaret kolonileri çağı ölü gömme adetleri. PhD, Gazi Üniversitesi, Ankara, Turkey (Unpublished PhD thesis, in Turkish with an abstract in English).

Erdal YS. (2011). Tasmasor Yakınçağ nekropolü ve iskeletlerinin antropolojik açıdan değerlendirilmesi. In: Şenyurt AY, editör. Tasmasor. Ankara: Bilgin Kültür Sanat Yayınları.

Erdal YS. (2013) Life and death at Hakemi Use. In: Nieuwenhuyse OP, Bernbeck R, Akkermans PMMG, J. Rogasch J, editors. Interpreting the Late Neolithic of Upper Mesopotamia. Brepols Publishers, Turnhout.

Esbensen KH. (2005) Multivariate data analysis in practice. Esbjerg, Denmark: 5th Edition, CAMO Process AS.

Grandfield K, Vuong V, Schwarcz HP. (2018) Ultrastructure of bone hierarchical features from nanometer to micrometer scale revealed in focused Ion beam sections in the TEM. Calcif Tissue Int 103(6):606–616.

Gonçalves D, Vassalo AR, Mamede AP, Makhoul C, Piga G, Cunha E, Marques MPM, Batista de Carvalho LAE. (2018) Crystal clear: vibrational spectroscopy reveals intrabone, intraskeleton, and interskeleton variation in human bones. Am J Phys Anthropol 166(2):296-312.

Gonçalves D, Thompson TJU, Cunha E. (2011) Implications of heat-induced changes in bone on the interpretation of funerary behaviour and practice. J Archaeol Sci 38(6):1308-1313.

GretagMacbeth. (2020) Munsell soil color charts, Revised washable edition. GretagMacbeth, New Windsor, NY.

Grunenwald A, Keyser C, Sautereau AM, Crubezy E, Ludes B, Drouet C. (2014) Revisiting carbonate quantification in apatite (bio)minerals: a validated FTIR methodology. J Archaeol Sci 49:134-141.

Hedges REM. (2002) Bone diagenesis: an overview of processes. Archaeometry 44(3):319-328.

Holden JL, Phakey PP, Clement JG. (1995) Scanning electron microscope observations of heat-treated human bone. Forensic Sci Int 74(1-2):29-45.

Hollund HI, Ariese F, Fernandes R, Jans MME, Kars H. (2013) Testing an alternative high-throughput tool for investigating bone diagenesis: FTIR in attenuated total reflection (ATR) mode. Archaeometry 55(3):507-532.

Işcan MY, Loth SR, Wright RK. (1984) Age estimation from the rib by phase analysis: white males. J Forensic Sci 29:1094-1104.

Işcan MY, Loth S R, Wright RK. (1985) Age estimation from the rib by phase analysis: white females. J Forensic Sci 30:853-863.

Kamış Y. (2012) Acemhöyük Erken Tunç Çağı Seramiği. PhD, Gazi Üniversitesi, Ankara, Turkey (Unpublished Ph. D thesis, in Turkish with an abstract in English).

Lebon M, Reiche I, Fröhlich F, Bahain JJ, Falguères C. (2008) Characterization of archaeological burnt bones: contribution of a new analytical protocol based on derivative FTIR spectroscopy and curve fitting of the v_1 v_3 PO_4 domain. 392(7):1479-1488.

Lebon M, Reiche I, Bahain JJ, Chadefaux C, Moigne AM, Fröhlich F, Sémah F, Schwarcz HP, Falguère C. (2010) New parameters for the characterization of diagenetic alterations and heat-induced changes of fossil bone mineral using fourier transform infrared spectrometry. J Archaeol Sci 37(9):2265-2276.

Lebon M, Müller K, Bellot-Gurlet L, Reche CP. (2011) Application des microspectrométries infrarouge et Raman à l'étude de sprocessus diagénéticques altérant les ossements paléollithiques. Archeosciences 35:179-190. (In French with an abstract in English).

Legan L, Leskovar T, Črešnar M, Cavalli F, Innocenti D, Ropret P. (2020) Non-invasive reflection FTIR characterization of archaeological burnt bones: reference database and case studies. J Cult Herit 41:13-26.

Lopes CCA, Limirio PHJO, Novais VR, Dechichi P. (2018) Fourier transform infrared spectroscopy (FTIR) application chemical characterization of enamel, dentin and bone. Appl Spectrosc Rev 53(9):747-769.

Lovejoy CO, Meindl RS, Pryzbeck TR, Meinsforth RP. (1985) Chronological metamorphosis of the auricular surface of the ilium: a new method for the determination of adult skeletal age at death. Am J Phys Anthropol 68:15-28.

Mamede AP, Gonçalves D, Marques MPM, Batista de Carvalho LAE. (2017) Burned bones tell their own stories: a review of methodological approaches to assess heat-induced diagenesis. Appl Spectrosc Rev 53(8):603-635.

Marshall AO, Marshall CP. (2015) Vibrational spectroscopy of fossils. Palaeontology 58(2):201-211.

Marques MPM, Mamede AP, Vassalo AR, Makhoul C, Cunha E, Gonçalves D, Parker SF, Batista de Carvalho LAE. (2018) Heat-induced bone diagenesis probed by vibrational spectroscopy. Sci Rep 8(1):1-13.

Meindl RS, Lovejoy CO. (1985) Ectocranial suture closure: a revised method for the determination of skeletal age at the death based on the lateral-anterior sutures. Am J Phys Anthropol 68:57-66.

Munro LE, Longstaffe FJ, White CD. (2007) Burning and boiling of modern deer bone: effects on crystallinity and oxygen isotope composition of bioapatite phosphate. Palaeogeogr Palaeoclimatol Palaoecol 249(1-2):90-102.

Nielsen-Marsh CM, Hedges REM. (2000) Patterns of diagenesis in bone I: the effects of site environments. J Archaeol Sci 27(12):1139-1150.

Olszta MJ, Cheng X, Jee SS, Kumar R, Kim Y, Kaufman MJ, Douglas EP, Gower LB. (2007) Bone structure and formation: a new perspective. Mater Sci Eng 58:77-116.

Özdemir K, Akyol AA, Erdal YS. (2015) A case of ancient bladder stones from Oluz Höyük, Amasya,

Turkey. Int J Osteoarchaeol 25:827–837.
Özgüç N. (1968) New light on the dating of the levels of the Karum of Kanish and of Acemhöyük near Aksaray. Am J Archaeol 318-320.
Öztan A. (1991) 1989 Yılı Acemhöyük Kazıları. Kazı Sonuçları Toplantısı 12(1):247-258.
Öztan A. (2014) 2013 Yılı Acemhöyük Kazıları ve Sonuçları. Kazı Sonuçları Toplantısı 36(2):61-72.
Person A, Bocherens H, Mariotti A, Renard M. (1996) Diagenetic evolution and experimental heating of bone phosphate. Palaeogeogr Palaeoclimatol Palaoecol 126:135–149.
Piga G, Gonçalves D, Thompson TJU, Brunetti A, Malgosa A, Enzo S. (2016) Understanding the crystallinity indices behavior of burned bones and teeth by ATR-IR and XRD in the presence of bioapatite mixed with other phosphate and carbonate phases. Int J Spectrosc 4810149:1-9.
Rey C, Renugopalakrishnan V, Collins B, Glimcher MJ. (1991) Fourier transform infrared spectroscopic study of the carbonate ions in bone mineral during aging. Calcif Tissue Int 49:251-258.
Rey C, Combes C, Drouet C, Glimcher MJ. (2009) Osteoporos bone mineral: update on chemical composition and structure. Osteoporos Int 20(6):1013-1021.
Rogers KD, Daniels P. (2002) An X-ray diffraction study of the effects of heat treatment on bone mineral microstructure. Biomaterials 23(12):2577-2585.
Roschger P, Paschalis EP, Fratzl P, Klaushofer K. (2008) Bone mineralization density distribution in health and disease. Bone 42(3):456-466.
Snoeck C, Lee-Thorp JA, Schulting RJ. (2014) From bone to ash: Compositional and structural changes in burned modern and archaeological bone. Palaeogeogr Palaeoclimatol Palaoecol 416:55-68.
Sözer, AN (1972). Kuzeydoğu Anadolu'da yaylacılık. Ankara: İş Matbaacılık.
Stathopoulou ET, Psycharis V, Chryssikos GD, Gionis V, Theodorou G. (2008) Bone diagenesis: new data from infrared spectroscopy and X-ray diffraction. Palaeogeogr Palaeoclimatol Palaeoecol 266(3-4):168-174.
Stiner, MC, Kuhn ST, Weiner S, Bar-Yosef O. (1995) Differential burning, recrystallization, and fragmentation of archaeological bone. J Archaeol Sci 22(2):223-237.
Surovell TA, Stiner MC. (2001) Standardizing infra-red measures of bone mineral crystallinity: an experimental approach. J Archaeol Sci 28(6):633-642.
Thompson TJU, Chudek JA. (2007) A novel approach to the visualisation of heat induced structural change in bone. Sci Justice 47(2):99-104.
Thompson TJU, Gauthier M, Islam M. (2009) The application of a new method of Fourier Transform Infrared Spectroscopy to the analysis of burned bone. J Archaeol Sci 36(3):910-914.
Thompson TJU, Islam M, Piduru K, Marcel A. (2011) An investigation into the internal and external variables acting on crystallinity index using Fourier transform infrared spectroscopy on unaltered and burned bone. Palaeogeogr Palaeoclimatol Palaoecol 299(1-2):168-74.
Thompson TJU, Islam M, Bonniere M. (2013) A new statistical approach for determining the crystallinity of heat-altered bone mineral from FTIR spectra. J Archaeol Sci 40:416-422.
Trueman CN, Tuross N. (2002) Trace elements in recent and fossil bone apatite. Rev Mineral and Geochem 48:489-521.
Trueman CN, Behrensmeyer AK, Tuross N, Weiner S. (2004) Mineralogical and compositional changes in bones exposed on soil surfaces in Amboseli National Park, Kenya: diagenetic mechanisms and the role of sediment pore fluids. J Archaeol Sci 31(6):721-739.
Ubelaker DH. (1989) Human skeletal remains: excavation, analysis, interpretation (Manuals on Archeology, 2). Taraxacum, Washington.
Van Strydonck M, Boudin M, De Muller G. (2010) The carbon origin of structural carbonate in bone apatite of cremated bones, Radiocarbon 52(2):578-586.
Von Euw S, Wang Y, Laurent G, Drouet C, Baboneau F, Nassif N, Azais T. (2019) Bone mineral: new insights into its chemical composition. Sci Rep 9(1):1-11.
Weiner S, Bar-Josef O. (1990) States of preservation of bones from the prehistoric sites in the Near East: a survey. J Archaeol Sci 17(2):187-196.
Weiner S, Wagner HD. (1998) The material bone: structure mechanical function relations. Annu Rev Mater Sci 28(1):271-298.
White TJ, Dong Z. (2003) Structural derivation and crystal chemistry of apatites. Acta Crystallogr B Struct Sci 59(1):1-16.
Wright LE, Schwarcz P. (1996) Infrared and isotopic evidence for diagenesis of bone apatite at Dos Pilas, Guatemala: palaeodietary implications. J Archaeol Sci 23(6):933-944.
Yalman B. (1996) 1994 Yılı İznik Roma Tiyatrosu Kazısı. Kazı Sonuçları Toplantısı 17(2):337–360.
Zazzo A, Lebon, M, Chiotti L, Comby C, Delqué-Količ E, Nespoulet R, Reiche I. (2013) Can we use calcined bones for ^{14}C dating the Paleolithic. Radiocarbon 55(3):1409-1421.